Experimental evidence of super-resolution better than λ/105 with positive refraction

Juan C Miñano[1], José Sánchez-Dehesa[2], Juan C González[1], P Benítez[1], D Grabovičkić[1], Jorge Carbonell[2] and H Ahmadpanahi[1]

[1] Universidad Politécnica de Madrid, Cedint, Campus de Montegancedo, 28223 Madrid, Spain
[2] Departamento de Ingenieria Electronica, Univ. Politécnica de Valencia, 46022, Valencia, Spain
E-mail: jcgonzalez@cedint.upm.es

Abstract

Super-resolution (SR) systems surpassing the Abbe diffraction limit have been theoretically and experimentally demonstrated using a number of different approaches and technologies: using materials with a negative refractive index, utilizing optical super-oscillation, using a resonant metalens, etc. However, recently it has been proved theoretically that in the Maxwell fish-eye lens (MFE), a device made of positive refractive index materials, the same phenomenon takes place. Moreover, using a simpler device equivalent to the MFE called the spherical geodesic waveguide (SGW), an SR of up to λ/3000 was simulated in COMSOL. Until now, only one piece of experimental evidence of SR with positive refraction has been reported (up to λ/5) for an MFE prototype working at microwave frequencies. Here, experimental results are presented for an SGW prototype showing an SR of up to λ/105. The SGW prototype consists of two concentric metallic spheres with an air space in between and two coaxial ports acting as an emitter and a receiver. The prototype has been analyzed in the range 1 GHz to 1.3 GHz.

Keywords: perfect imaging, super-resolution, spherical geodesic waveguide

1. Introduction

Ernst Abbe, in 1873, found that the minimum size of the spot that can be focused with a conventional optical system is limited to the wavelength of the radiation, a phenomenon known as the diffraction limit. This size is called the resolution of the optical instrument and corresponds to the well-known expression: $d = 1.22\lambda/(2NA)$, where d is the diameter of the spot, λ the wavelength, and NA the numerical aperture of the objective. The attenuation of the evanescent waves in far field with the loss of information transported by these waves is the physical cause of the diffraction limit. Numerous works have been devoted to overcome this limit, called super-resolution (SR), mostly based on capturing the evanescent waves and then focusing them together with transmitted waves. The capture of evanescent waves was first proposed by Synge in 1928 [1] while the first experimental device demonstrating resolutions below the diffraction limits, the near-field optical microscopy, was developed in 1984 [2, 3]. Fluorescence based imaging methods and resonant metalenses are proposed alternatives that use the evanescent waves recovering to reach SR imaging [4, 5]. Another approach used to achieve super-resolution by recovering evanescent waves is that of the negative refraction lens [6]. Contrary to other evanescent recovering methods, the lens does not have to be placed to a sub-wavelength distance from the object, that is, it is in theory a far field lens. Unfortunately, high absorption and, in consequence, small (wavelength scale) source-to-lens distance are necessary. In fact, it was claimed in [7] that this is inevitable with real negative refraction materials, although recent arguments rebut it [8].

Clearly, it is important for us to design an SR system where the distance between the object and lens is higher, facilitating the manufacture and development of practical SR devices. The most promising solution is the use of an optical super-oscillations system [9]. The concept of super-oscillation was first proposed by Torraldo di Francia [10] as one adaptation of the well known super-directive microwaves antennas to optical frequencies. In the classical devices the object emits radiation that firstly travels through free space or another medium before arriving at the optical system, then passes through the optics and finally again through the free space to reach the image. To avoid decay of the evanescent waves in free space (outside the optical system) the object and image have to be placed very close to the optical system. The super-oscillating system works in a completely different way. The radiation is focused on a sub-wavelength area of the sample, from where it is redirected and collected using conventional lenses. Scanning over the complete sample, a SR image can be obtained. Experimental SR better than $\lambda/6$ has been presented, showing this technology to be a good candidate for the future development of SR systems. At this moment the very low efficiency and the difficulties of manufacturing are the most important challenges to be solved [9].

Another alternative device for super-resolution was proposed in 2009 [11, 12]: the Maxwell fish eye (MFE) lens. This device is very well known in the framework of geometrical optics because it is an absolute instrument [13], meaning that every object point has a stigmatic image point. In the case of an MFE lens, the source and image are placed inside the lens. The principal difference between this and previous solutions is that the radiation emitted by the source does not travel through free space. It is well known that the classical waveguide with linear symmetry has a complete set of modes where some of them are evanescent in the direction of the symmetry axis. For a waveguide without linear symmetry, like the MFE, this conditions is not necessary, thus in theory, the problem of evanescent decay may not exist in

these structures. However this theoretical study of evanescent modes has not been realized yet, and will be a task for a future work.

Leonhardt [11] analyzed Helmholtz wave fields in the MFE lens in two dimensions (2D). These Helmholtz wave fields describe TE-polarized modes in a cylindrical MFE, i.e., modes in which an electric field vector points orthogonally to the cross section of the cylinder. Leonhardt found a family of Helmholtz wave fields which have a monopole asymptotic behavior at an object point as well as at its stigmatic image point. Each one of these solutions describes a wave propagating from the object point to the image point. It coincides asymptotically with an outward (monopole) Helmholtz wave at the object point, as generated by a point source, and with an inward (monopole) wave at the image point, as it was sunk by an 'infinitely-well localized drain' (which we call a 'perfect point drain'), a result that has also been confirmed via a different approach [14]. This perfect point drain absorbs the incident wave with no reflection or scattering.

In [11] Leonhardt analyzed the behavior of the system when the drain was placed at the image point, but he did not analyze the cases in which the drain is displaced from that image point. This was carried out later with COMSOL simulations using perfect conductors, which showed SR up to $\lambda/500$ using imperfect drains in 2011 [15] and up to $\lambda/3000$ using perfect drains in 2012 [16] (note that it is not necessary to use a perfect drain to achieve a SR). These simulations were carried out on the spherical geodesic waveguide (SGW), a device equivalent to the MFE proposed in [17], which is a spherical waveguide filled with a non-magnetic material and isotropic refractive index distribution proportional to $1/r$ ($\varepsilon(r) = (r_0/r)^2$ and $\mu = 1$), r being the distance to the center of the spheres. The equivalence between the MFE and the SGW was demonstrated using transformation optics theory, so the TE-polarized electric modes of the cylindrical MFE [11] are transformed into radial-polarized modes in the SGW [17]. In the SGW, the object and image points are just antipodal points.

The first experiment to demonstrate the SR capability in the MFE was carried out at a microwave frequency ($\lambda = 3\,\text{cm}$) [18]. A two-dimensional MFE medium was assembled as a 5 mm thick planar waveguide with concentric layers of copper circuit board and dielectric fillers forming the desired refractive index profile of the MFE. Sources and drains were built as coaxial ports loaded by characteristic impedance, which is not a perfect drain. The experimental results showed that two sources with a distance of $\lambda/5$ from each other (where λ denotes the local wavelength $\lambda = \lambda_0/n$) could be resolved.

The theoretical analysis of the MFE in [11] and the simulations of the SGW in [15] and [16] showed that these two structures with positive refraction are a good alternative. The experimental results for the MFE confirmed this result; however the $\lambda/5$ SR measured so far is rather close to the Abbe limit (which for the MFE is $\sim\lambda/3$ [18]) and it has been achieved only for one wavelength.

Here, novel experimental results for a SGW prototype are presented showing an SR of up to $\lambda/105$ for a set of specific frequencies and loads. The measurements have been made for a wide range of frequencies (1.0 GHz–1.3 GHz).

Note that here the definition of SR is different from the classical SR definition which is used in other previously mentioned approaches and generally in optics, where SR is defined as the minimum size of the spot that can be obtained in the imaging. In this paper the SR is defined as the minimum displacement of a point receptor that causes a drop of the power to 10% of the value received in the initial position.
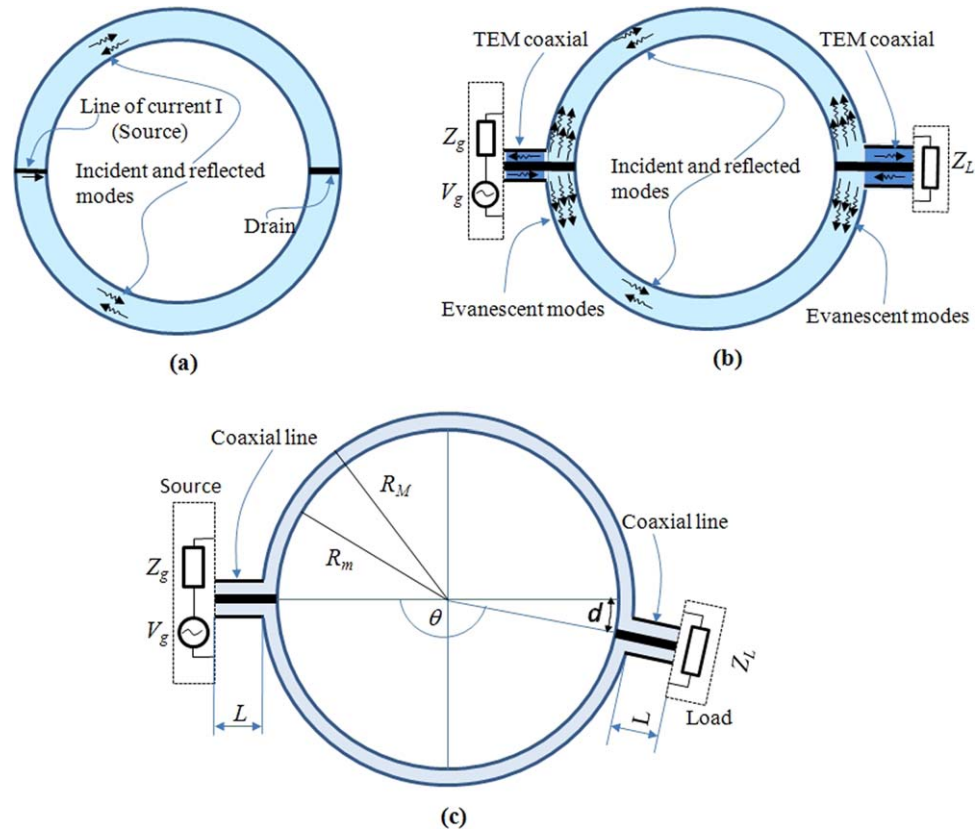
Figure 1. Microwave (a) SGW with a current line source and a line drain located at the antipodal position. (b) SGW with the source implemented as input coaxial ports with a voltage generator V_G and an impedance Z_G, and the drain implemented as an output coaxial port loaded with an impedance Z_L. (c) Concept of super-resolution in the SGW: the drain is displaced an arc length of λ/N from the antipodal position of the source and the output power is measured at each position.

The paper covers all the steps from the design to the characterization of the prototype: first, the description of the system and the theoretical background; second, simulations of an ideal SGW and of a real model are carried out with COMSOL multiphysics; third, a description of the prototype and the analysis of the measurements showing results in complete agreement with the simulations; and finally an optimization of the appropriate drain for the system to obtain an SR of up to $\lambda/105$.

2. Description of the system

Figure 1(a) presents the cross sectional scheme of the ideal SGW model with the same imaging properties as the MFE, previously analyzed by Leonhardt [11]. The system consists of a source, which is a current line, the SGW made up of two metallic concentric spherical shells and a drain, an absorbing line. The ideal source and drain are difficult to manufacture so here a different way of introducing and extracting the power is used (figure 1(b)). The source is made up of a voltage source V_G, an impedance Z_G and a single mode input coaxial port which connects to the SGW spheres. The drain is an analogue output coaxial port loaded with an
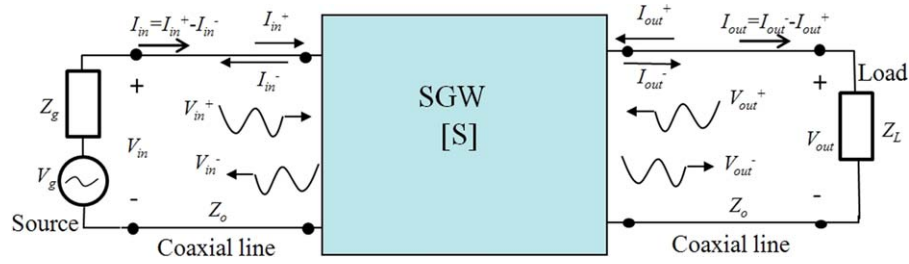
Figure 2. Microwave circuit model of the SGW system.

impedance Z_L. For an arbitrary impedance Z_L, a reflected mode will propagate backwards towards the source, as indicated in figure 1(b). There is a Z_L value that cancels out that reflected mode [16], emulating the perfect drain described by Leonhardt [11]. In this paper super-resolution will be analyzed as a function of Z_L. The model in figure 1(b) has two advantages over that shown in figure 1(a): it is easier to manufacture and the classic theory of microwave circuits can be applied, particularly the characterization by means of a matrix of dispersion parameters ([S] matrix).

Figure 1(c) describes the concept of super-resolution used here, first introduced in [15] and [16]. The analysis of SR is carried out as follows:

- First, a Z_L is selected.
- Second, for this Z_L in the opposite pole ($\theta = \pi$), the impedance seen by the generator (to the right of the generator in figure 1) is obtained, Z_{in}. This is done using the [S] matrix formalism (see below).
- Third, Z_G is selected to maximize the injection of power in the SGW, that is $Z_G = Z_{in}*$.

Finally, the drain is displaced from the antipodal position with respect to the source by a shift of arc length d. The parameter used to characterize the SR is M_{ZL}, defined as:

$$M_{Z_L}(d) = \frac{P_{Z_L}(d)}{P_{Z_L}(0)} \tag{1}$$

where $P_{ZL}(d)$, is the power delivered to the load when the drain is displaced from the opposite pole by a distance d.

We define the 'resolution' as the arc length d (expressed in wavelength units) for which $M_{ZL}(d) = 0.1$. This is not very different from the Rayleigh criterion in optics, which refers to the first null.

The parameter M_{ZL} is not directly measured by the test equipment. The equipment gives the scattering matrix [S] at the input and output ports defined respectively by the coaxial source and drain ports. This matrix is used to calculate the parameter M_{ZL}, as described in the Methods section.

2.1. Scattering matrix

In this paper and in [15, 16], the classic theory of microwave circuits is used for the super-resolution analysis (see [15, 19]), see figure 2.

The [S] matrix permits us to calculate the parameter M_{ZL} for every pair of impedances Z_G and Z_L. The power delivered to the load is:
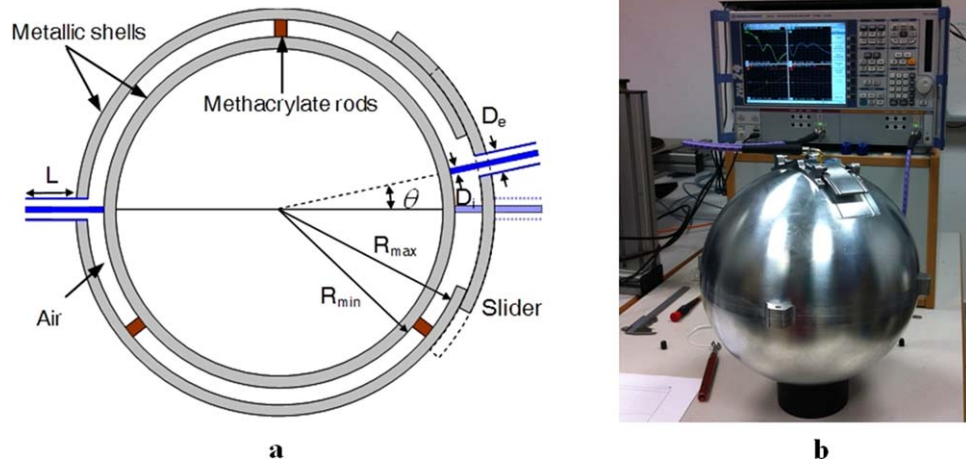
Figure 3 (a) Schematic presentation of the spherical geodesic waveguide (SGW) with coaxial cables (blue color), the gray color corresponds to the metallic conductive walls (aluminum) and white color corresponds to the dielectric waveguide. The slider is moving smoothly on the outer sphere to tilt the drain position. (b) Experimental setup. The SGW is connected to the ZVA 24 vector network analyzer (VNA) through coaxial cables.

$$P_{ZL} = \frac{|V_g|^2}{2} \frac{|Z_{in}|^2}{|Z_g + Z_{in}|^2} \frac{\mathrm{Re}[Z_L]}{|Z_L|^2} |H|^2$$

$$H = \frac{V_{out}}{V_{in}} = \frac{V_{out}^+ + V_{out}^-}{V_{in}^+ + V_{in}^-} \tag{2}$$

Where H and Z_{in} are obtained from the equations:

$$\begin{bmatrix} V_{in}^- \\ V_{out}^- \end{bmatrix} = \begin{bmatrix} S_{11} & S_{12} \\ S_{21} & S_{22} \end{bmatrix} \begin{bmatrix} V_{in}^+ \\ V_{out}^+ \end{bmatrix} \quad \frac{V_{out}^+ + V_{out}^-}{V_{out}^- - V_{out}^+} Z_0 = Z_L \quad Z_{in} = \frac{V_{in}^+ + V_{in}^-}{V_{in}^+ - V_{in}^-} Z_0 \tag{3}$$

The ratio between the power delivered to the drain loaded by an impedance Z_L when it is displaced from its initial position, with respect to the power delivered to the same load placed at its initial position, i.e. at the antipode point, is given as:

$$M_{Z_L} = \frac{P_{ZLd}}{P_{ZLo}} = \frac{|H_d|^2}{|H_o|^2} \frac{|Z_g + Z_{ino}|^2}{|Z_g + Z_{ind}|^2} \frac{|Z_{ind}|^2}{|Z_{ino}|^2} \tag{4}$$

where the subscripts d and o refer to the different drain positions, when it is displaced and at the antipode position, respectively

2.2. Manufactured SGW

Figure 3(a) presents the scheme of the manufactured SGW. The source is fixed, while the drain is connected with a moveable slider. The source and the drain are much smaller than the SGW, hence they can be considered as a good approximation of the point source and drain.

The SGW dimensions are $R_{max} = 150$ mm, $R_{min} = 145$ mm (which is six times smaller than the SGW from [15, 16], while the air filled thickness remains the same at 5 mm), $D_i = 1.3$ mm (diameter of the inner coaxial line), $D_e = 4.1$ mm (diameter of the outer coaxial line), $L = 10$ mm. The conductive walls are made of aluminum with thickness of 10 mm. The thickness of the air filled waveguide is 5 mm, which is equal to the height of the methacrylate rods (red rods in figure 3(a)).

Figure 3(b) illustrates the experimental setup for the measurement. The source and the drain are two SMA connectors that have been fixed to the SGW with screws. The scattering parameters were measured directly using a vector network analyzer (VNA) from Rohde & Schwarz (ZVA 24).

2.3. Simulations using COMSOL multiphysics

The simulation has been carried out using the 3D RF module in COMSOL Multiphysics. Using this COMSOL package, a realistic model of the SGW prototype has been designed. The model includes all additional pieces (such as the slider, holder, methacrilate rods, etc) as shown in figure 3(a). Dimensions and properties of all the objects are the same as in the prototype (see section 2.2).

Special care has been taken to define the mesh of the system. In order to mesh the waveguide properly, the geometry has been divided into several domains. Each domain is meshed separately according to its geometric and physical properties. Since the waveguide thickness is very small ($(R_{max} - R_m)/R_m \ll 1$), the SGW is meshed using a swept mesh (2D triangular mesh from the outer shell is swept to the inner shell). The coaxial cables have a higher density mesh, using 3D tetrahedra. The mesh density is increased since the change variation of the electrical field is significant in the neighborhood of the coaxial probes. Furthermore, abrupt transitions between different pieces are meshed with a higher density in order to account for their influence on the results.

3. Results

The results are separated into three parts. Firstly, the scattering matrix [S] is presented, as measured and simulated with COMSOL Multiphysics, which are in complete agreement. The simulation takes into account all the features of the manufactured SGW (holders of the inner sphere, spacers, slider to displace the drain probe position), and properties of real materials (aluminum for the SGW shells, teflon and gold for the coaxial connectors). Secondly, the parameter M_{ZL} is computed for the measured and simulated matrices [S], and additionally, for comparison purposes, it is also computed for another simulated matrix [S] in which the model considers the metals as perfect conductors and does not include additional features of the manufactured SGW. Finally, in the third part, the results obtained with optimal impedances Z_L and Z_G, which maximize the super-resolution, are presented.

In order to verify the precision of the experiment, we have compared measured scattering parameters (i.e., the coefficients of the matrix [S]) with those obtained using a COMSOL simulation. Consider, for example, the scattering parameter S_{21} (usually referred to as the transmission coefficient). When the output coaxial port is loaded with $Z_L = Z_0$, the characteristic impedance of the coaxial cables, the power delivered to the drain is proportional to $|S_{21}|^2$ ($|S_{21}|^2 = P_{Z0}/P_{ag}$) where P_{ag} is the maximum power that can be delivered by the generator.
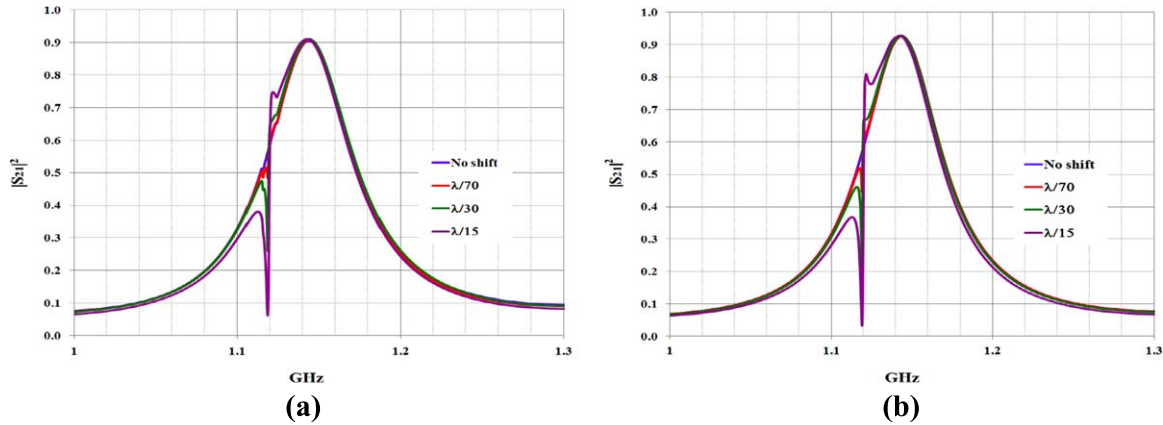
Figure 4. Magnitude of the scattering parameter S_{21} measured in the experiment (figure (a)) and simulated in COMSOL (figure (b)). In the graphs, the squared value $|S_{21}|^2$ is given, since it is directly related to the delivered power. The position of the notch frequency is similar, but the simulated notch is slightly deeper than the measured one.

Figure 4 shows the $|S_{21}|^2$ for different displacements and for the range of frequencies considered in the experiment (from 1 GHz to 1.3 GHz). The blue curve represents the results obtained when the output coaxial port is in the antipodal position, while other colors correspond to different shifts ranging from $\lambda/15$ to $\lambda/70$. Figure 4(a) presents the experimental results, while figure 4(b) shows the simulated ones. According to the graphs, one can see a great level of coincidence between the results.

Figure 5 shows the computed M_{Z0}, that is, M_{ZL} when $Z_L = Z_0$ for different positions of the output coaxial port and different frequencies for three different cases. Figure 5(a) and figure 5(b) correspond to the matrix [S] obtained using a COMSOL simulation with perfect conductors. Figure 5(c) and figure 5(d) correspond to the matrix [S] obtained with a COMSOL simulation with realistic conductor parameters and all the additional pieces from the prototype. Figure 5(e) and figure 5(f) correspond to the matrix [S] measured experimentally. In the figures on the left, the abscissa axis is the frequency and the label of each curve indicates the shift in the output coaxial port, which is how it is obtained from COMSOL. In the figures on the right, the abscissa axis is the shift (expressed in units of λ) and the labels indicate different frequencies, which is more convenient to visualize the super-resolution properties.

In the left-hand graphs in figure 5, the blue curve corresponds to the coaxial port placed on the antipode (which is thus equal to 1) while the other curves correspond to different shifts, which are in all cases much smaller than the wavelength, from $\lambda/15$ to $\lambda/210$. The minimum M_{Z0} value is obtained for all shifts at $f = 1.120\,744$ GHz in the lossless case (figure 5(a)) and at $f = 1.119\,16$ GHz for the real model, which correspond to $\lambda = 267.68$ mm and $\lambda = 268.06$ mm, respectively. These frequencies are called notch frequencies and are close to the Schumann resonance frequencies of the sphere [15].

In the right-hand graphs in figure 5, the resolution for different frequencies when $Z_L = Z_0$ for the three cases (lossless simulation, realistic simulation, and measurements) can be computed, as defined previously, by searching the shift at which M_{Z0} drops to 0.1. With this definition, at the notch frequency (the blue curve on the right figures) the resolution is $\lambda/250$ for the lossless simulation, $\lambda/18$ for the realistic simulation and $\lambda/15$ for the measured case.
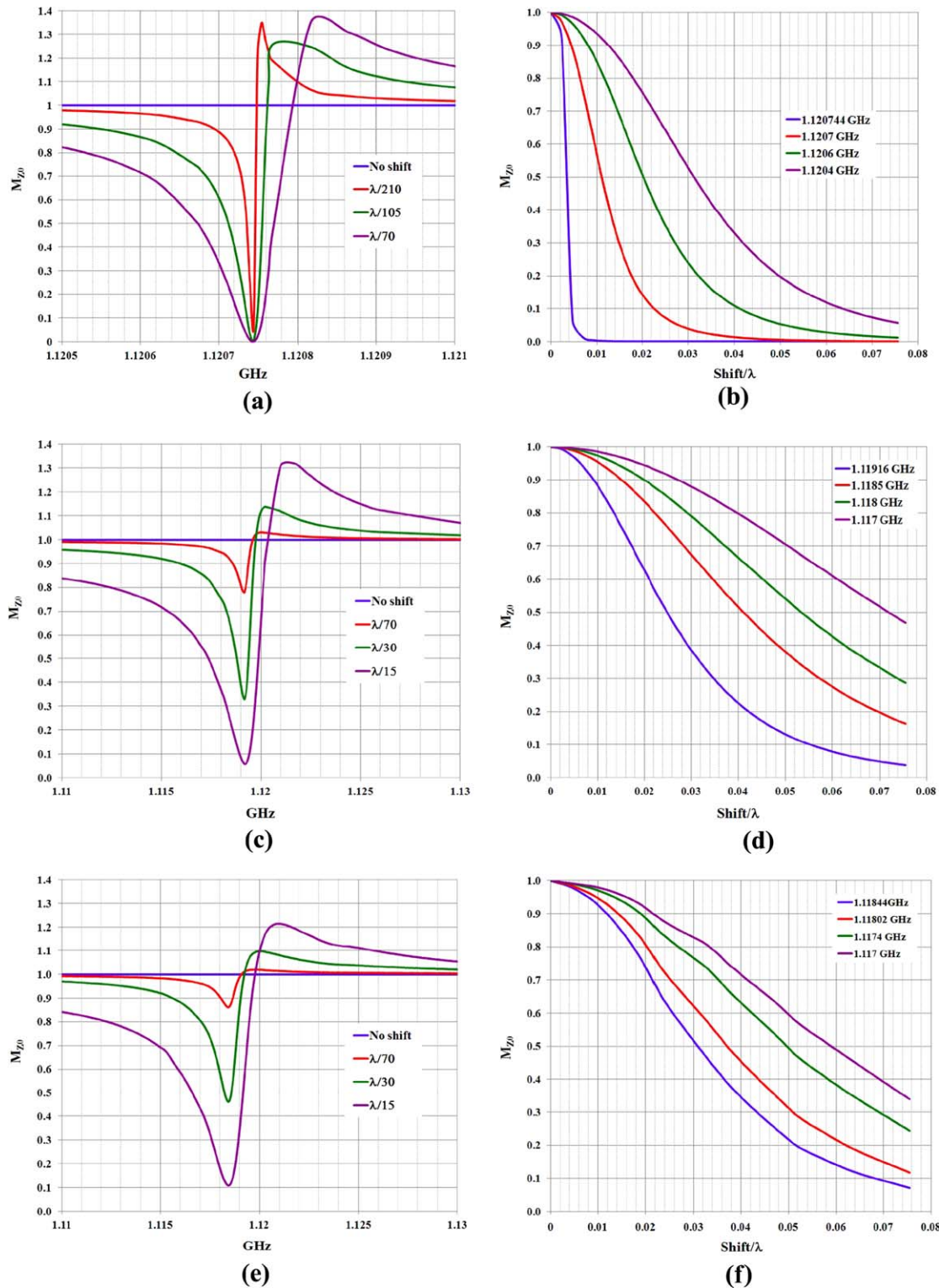
Figure 5. M_{Z0} as function of the frequency and the output port shift calculated for the matrices [S] obtained by: (a), (b) a COMSOL simulation assuming perfect conductors, (c), (d) a COMSOL simulation with realistic conductor parameters, (e), (f) experimental measurements of the prototype.

Outside the notch frequency the super-resolution decreases, for example at 1.1204 GHz it is $\lambda/15$ for the lossless case (the violet curve in figure 5(b)).

The measured and realistically simulated results agree very well (figures 5(c), (d) and figures 5(e), (f)), with the measured super-resolution at the notch frequency only slightly smaller than the simulated one ($\lambda/15$ versus $\lambda/18$). On the other hand, the simulations show that the metal losses are responsible for a significant drop in super-resolution, from $\lambda/250$ to $\lambda/18$.

These resolution values correspond to the case in which $Z_L = Z_0$, which may not be the optimum case for obtaining the highest resolutions. The parameter M_{ZL} can be calculated for different complex Z_L values, finding their notch frequencies, and computing their resolutions for comparison.

Figure 6(a) and figure 6(c) show M_{ZL} at the notch frequency obtained with the measured matrix [S] as a function of the complex values of Z_L for two different output port shifts with respect to the antipodal position ($\lambda/105$ in figure 6(a) and $\lambda/42$ in figure 6(c)). The surface $M_{ZL}(\text{Re}[Z_L], \text{Im}[Z_L])$ is represented in two colors: the blue portion shows the region with $M_{ZL} < 0.1$ and the red one corresponds to the regions with $M_{ZL} > 0.1$. This means that the blue region defines the set of impedances Z_L providing a super-resolution higher than $\lambda/105$ in figure 6(a) and higher than $\lambda/42$ in figure 6(c).

Another important parameter to take into account is the efficiency (see figure 1(c)), defined as the ratio of $P_{ZL}(0)/P_{ag}$ (P_{ag} is the maximum power that can be delivered by the generator). Figure 6(b) and figure 6(d) represent the efficiency of the system for the same respective shifts, $\lambda/105$ and $\lambda/42$.

The region in which the higher super-resolution is found corresponds to smaller values of the real part of Z_L. The efficiency in that region is, however, also lower, implying the power of the generator is being significantly lost through dissipation in the metals.

Besides that region of high super-resolution with smaller values of the real part of Z_L, super-resolution is also achieved for greater values of Z_L real and imaginary parts (for example for $Z_L = 1000 + {}^i*1000$), which are not shown in figure 6. However, for these values of Z_L the highest super-resolution achieved is $\lambda/42$ and the efficiency is lower than in the case presented in figure 6 (only 40%, which is much lower than the efficiency obtained for $\lambda/42$ super-resolution from figure 6(d), which was 80%).

Figure 7(a) shows the maximum efficiency for all the measured displacements. The results are obtained using low values of the real part of Z_L (the same as in figure 6). During the experiment the drain has been displaced to 25 different positions. The minimum displacement was $\lambda/420$, while the maximum was $\lambda/13$. The graph from figure 7(a) starts at the shift $\lambda/105$, since it is the smallest displacement for which the super-resolution is achieved. For super-resolution worse than $\lambda/25$, the efficiency is practically constant at about 94%. Figure 7(b) shows the loci of the Z_L values in the complex plane at which these maximum efficiencies are obtained. The labels indicate the resolution values attained at several Z_L values.

4. Discussion

Leonhardt, in [11] and [12], suggested that MFE, a positive refraction device, should produce SR for any frequency using perfect drains. Subsequent results showed that SR does take place but with two differences with respect to Leonhardt's theory: firstly, in the experiments with the MFE [18] and simulations with the SGW [12] SR has been achieved without using the perfect
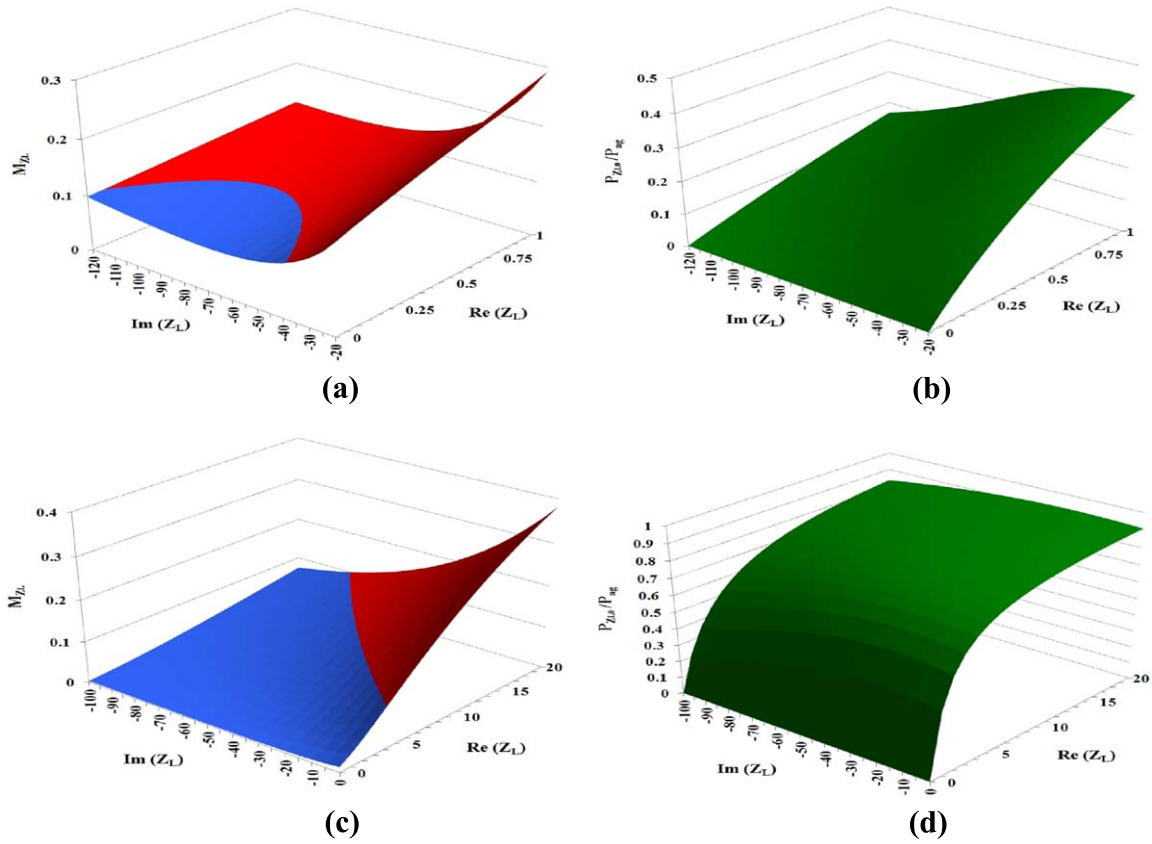
Figure 6. Finding Z_L for maximum super-resolution with the measured matrix [S]. (a) M_{ZL} when the drain is shifted by $\lambda/105$ as a function of Z_L. (b) Efficiency for the same range of Z_L values as in figures 5(a), (c) M_{ZL} when the drain is shifted by $\lambda/42$ as a function of Z_L. (d) Efficiency for the same range of values of Z_L as in figure 3(c).
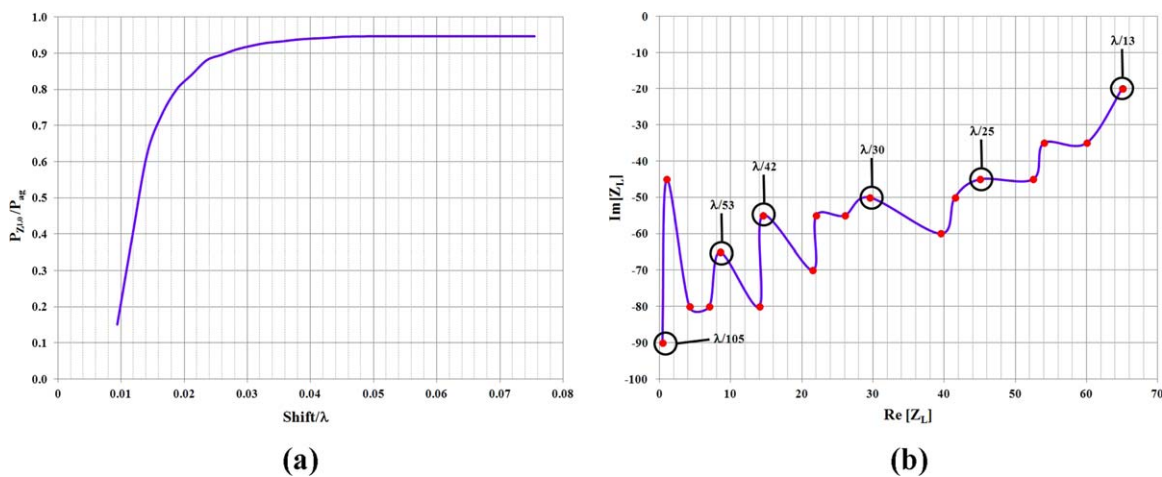
Figure 7. Efficiency obtained for different SR figures. The value of the abscissa denotes achieved SR expressed in λ. (b) Z_L values providing those maximum efficiencies.

drain; secondly, SR happens only in a narrow band of frequencies. In [18] and [15], the drain is made up of coaxial ports loaded with their characteristic impedances, so the absorption of the incident wave is not perfect. Later, simulations of the SGW using the perfect drain were carried out as well [16]. Although the SR level increases from $\lambda/500$ to $\lambda/3000$, the perfect drain does not significantly change the band of frequencies in which SR takes place. In [18] experimental evidence of SR using an MFE was demonstrated; however, only $\lambda/5$ resolution was achieved for a specific microwave frequency. The experimental results presented here demonstrate a high level of SR (up to $\lambda/105$) with a positive refraction device for the first time. The results are in complete accordance with the simulation. It is shown that SR only takes place in a narrow band of frequencies and depends significantly on the receptor used. In order to obtain an efficient device providing a high SR, it is not necessary to use the perfect drain.

Experimental results for the MFE presented in [11, 18], simulations for the SGW in [15, 16] and the work presented here represent the first step in understanding the possibilities of a super-resolution system based on waveguides. In order to develop an imaging system based on the SGW a deeper modal analysis is necessary in order to define conditions necessary for image formation. Some results have been presented in [20] but some fundamental mathematical and conceptual problems are not yet solved.

Acknowledgments

References

[1] Synge E H 1928 A suggested method for extending microscopic resolution into the ultramicroscopic region *Phil. Mag.* **6** 356–62

[2] Pohl D W, Denk W and Lanz M 1984 Optical stethoscopy: image recording with resolution $\lambda/20$ *Appl. Phys. Lett.* **44** 651

[3] Lewis A, Isaacson M, Harootunian A and Muray A 1984 Develpoment of a 500 Å spatial resolution light microscope *Ultramicroscopy* **13** 227–31

[4] Hell S W and Wichman J 1994 Breaking the diffraction resolution limit by stimulated emission: stimulated-emission-depletion fluorescence microswcopy *Opt. Lett.* **19** 780

[5] Lemoult F, Lerosey G, de Rosny J and Fink M 2010 Resonant metalenses for breaking the diffraction barrier *Phys. Rev. Lett.* **104** 203901

[6] Pendry J B 2000 Negative refraction makes a perfect lens *Phy. Review Let.* **85** 3966–89

[7] Stockman M I 2007 Criterion for negative refraction with low optical losses from a fundamental principle of causality *Phys. Rev. Lett.* **98** 177404

[8] Kinsler P and McCall M W 2008 Causality-based criteria for a negative refractive index must be used with care *Phys. Rev. Lett.* **101** 167401

[9] Rogers E T F and Zheludev N I 2013 Optical super-oscillations: sub-wavelength light focusing and super-resolution imaging *J. Opt.* **15** 094008

[10] di Francia T G 1952 Super-gain antennas and optical resolving power *Nuovo Cimento Suppl.* **9** 426–35

[11] Leonhardt U 2009 Perfect imaging without negative refraction *New J. Phys.* **11** 093040

[12] Leonhardt U and Philbin T G 2010 Perfect imaging with positive refraction in three dimensions *Phys. Rev.* A **81** 011804

[13] Born and Wolf E 1998 *Principles of Optics* 6th edn (Cambridge: Cambridge University Press) p 143

[14] Benítez P, Miñano J C and González J C 2010 Perfect focusing of scalar wave fields in three dimensions *Opt. Express* **18** 7650–63

[15] Miñano J C, Marqués R, González J C, Benítez P, Delgado V, Grabovickic D and Freire M 2011 Super-resolution for a point source better than $\lambda/500$ using positive refraction *New J. Phys.* **13** 125009

[16] González J C, Grabovickic D, Benítez P and Miñano J C 2011 Circuital model for the spherical geodesic waveguide perfect drain *New J. Phys.* **14** 083033

[17] Miñano J C, Benítez P and González J C 2010 Perfect imaging with geodesic waveguides *New J. Phys.* **12** 123023

[18] Ma Y G, Sahebdivan S, Ong C K, Tyc T and Leonhardt U 2010 Evidence for subwavelength imaging with positive refraction *New J. Phys.* **13** 033016

[19] Pozar D M 2005 *Microwave Engineering* (New York: Wiley) p 196

[20] González J C, Benítez P, Miñano J C and Grabovickic D 2012 Perfect imaging analysis of the spherical geodesic waveguide *Proc. SPIE* **8550** 12